Journal of Materials Chemistry C

Self-standing and shape-memorable UV-curing epoxy for three-dimensional (3D) continuous-filament printing

Journal:	*Journal of Materials Chemistry C*
Manuscript ID	TC-ART-10-2017-004873.R1
Article Type:	Paper
Date Submitted by the Author:	22-Jan-2018

Complete List of Authors:	Sun, Hanna; Sungkyunkwan University, Suwon, South Korea, Department of Energy Science Kim, Youngjun; Sungkyunkwan University, Suwon, South Korea, School of Chemical Engineering, Department of Polymer Science and Engineering Kim, Ye-Chan; Sungkyunkwan University, Suwon, South Korea, Department of Energy Science Park, In-Kyung; Sungkyunkwan University, Suwon, South Korea, School of Chemical Engineering, Department of Polymer Science and Engineering Suhr, Jonghwan; Sungkyunkwan University, Department of Polymer Science and Engineering; Sungkyunkwan University, Suwon, South Korea, Department of Energy Science; Sungkyunkwan University, Suwon, South Korea, Department of Mechanical Engineering Byun, Doyoung; Sungkyunkwan University, Mechanical Engineering Kuk, Keon; Samsung Electronics Co, Ltd., DMC R&D Center Baek, Oh-Hyun; Samsung Electronics Co, Ltd., DMC R&D Center Jung, Yeon-Kyung; Samsung Electronics Co, Ltd., DMC R&D Center Choi, Hyoung; Inha University, Department of Polymer Science and Engineering Kim, Kwang; University of Nevada, Las Vegas, Mechanical Engineering Department Nam, Jae-Do; Sungkyunkwan University, Suwon, South Korea, Department of Energy Science; Sungkyunkwan University, Suwon, South Korea, School of Chemical Engineering, Department of Polymer Science and Engineering

Journal of Materials Chemistry C

PAPER

Self-standing and shape-memorable UV-curing epoxy for three-dimensional (3D) continuous-filament printing

Received 25th October 2017,
Accepted 00th January 20xx

DOI: 10.1039/x0xx00000x

www.rsc.org/

H. Sun,[a] Y. Kim,[b] Y. C. Kim,[a] I. K. Park,[b] J. Suhr,[a,b,c] D. Byun,[c] K. Keon,[d] O. H. Baek,[d] Y. K. Jung,[d] H. J. Choi,[e] K. J. Kim[f] and J. D. Nam[a,b*]

In the development of three-dimensional printable materials for high-speed and high-resolution printing, UV-curing polymers can guarantee a fast and precise printing of high performance load-bearing structures, but the injected drops of the monomers tend to spread over the substrates due to their low viscosity. In this study, we imposed self-standing and shape-memorable capability to an epoxy acrylate (EA) monomer to ensure a continuous filamentary 3D printing while maintaining its low viscosity nature. Using octadecanamide (ODA) with EA, the strong hydrogen-bond networks (-N-H···O=C-, -N-C=O···H-O-, -N-H···N-) was additionally achieved in the material system and the developed material distinctively exhibited rheological duality in different processing stages: Low-viscosity liquid-like behavior (~50 Pa·s of viscosity) while passing through the nozzle, and self-standing solid-like behavior (~364 Pa of static yield stress) right after being printed. This reversible liquid-to-solid transitional capability was quantified by viscoelastic complex moduli providing a dynamic yield stress ($\tau_{y,G}$) as 210 Pa corresponding to the upright stacking up to ca. 3.2 cm (3 wt% of ODA). The time ($t_{y,G}$) required for the conformational rearrangement was evaluated as fast as ca. 10-2 sec. After UV curing, the 3D printed layers exhibited no air pockets or weld lines at the stacked interfaces, which could guarantee excellent mechanical performance and structural integrity.

Introduction

Three-dimensional (3D) printing is a promising fabrication technology that attracts a great deal of attention in the manufacturing fields ranging from aerospace and automotive to bioengineering.[1-4] This additive manufacturing method offers almost unlimited and unconstrained structures in a customized way without using molds, which can hardly be achieved by the traditional subtractive manufacturing technology.[5-9] As 3D printing becomes more and more central in the small-scale manufacturing fields, versatile 3D-printable inks are urgently needed to achieve not only feasible processing characteristics for fast printing but also robust structural properties for being used in load-bearing structures.[10-12] Currently, the 3D printing methods may be classified into two main categories in light of feedstock materials: continuous-filament and drop-jetting 3D printing.

The continuous-filament printing commonly uses thermoplastic polymers as a feedstock. It allows a rapid fabrication of 3D structures (*ca*. 5-15 cm/hr in the *Z*-axis), where the extruded filaments quickly solidify to construct the shapes.[13] However, the viscosity of its feedstock thermoplastics is usually high in the printing region of shear rate (e.g., ~10^3 Pa·s for PLA), which inevitably requires large nozzle diameter (>250 μm) resulting in poor resolution of final products.[14, 15] On the other hand, the drop-jetting 3D printing usually adopts low-viscosity thermosetting monomers (most commonly UV-curable acrylates), which desirably allows a small nozzle size and high-resolution printing. However, the jetted droplets of thermoset monomers (1-5 μm diameter droplets) usually tend to spread over the substrate resulting in poor stacking capability (i.e., low aspect ratio of the injected drops) and low printing speeds (*ca*. ~3 cm/hr in the *Z*-axis in commercial machines).[16-19] Accordingly, if an upright standing capability is imposed to those thermoset monomers, a continuous-filamentary printing could be ensured in the 3D printing of thermoset monomers, which may not only overcome the poor stacking capability of drop-jetting 3D printing but also achieve higher resolution than continuous-filament printing. Our work, therefore, focuses on ensuring a continuous-filament printing using a thermoset-monomer feedstock, which allows small nozzle size and high printing speed.

Recent work has focused on controlling the rheological behaviours of 3D printing materials to apply the desired methods including the continuous-filament and drop-jetting

[a] *Department of Energy Science, Sungkyunkwan University, Suwon 16419, Republic of Korea. E-mail: jdnam@skku.edu*
[b] *School of Chemical Engineering, Department of Polymer Science and Engineering, Sungkyunkwan University Suwon 16419, Republic of Korea.*
[c] *Departmen of Mechanical Engineering, Sungkyunkwan University, Suwon 16419, Republic of Korea.*
[d] *DMC R&D Center, Samsung Electronics Co, Ltd., Seoul 06765, Republic of Korea*
[e, 5] *Department of Polymer Science and Engineering, Inha University, Incheon 22212, Republic of Korea*
[f, 6] *Department of Mechanical Engineering, University of Nevada, Las Vegas, 4505 S.Maryland Parkway, Las Vegas, NV 89154, United State*

3D printing. Especially, for the direct-write printing, shear-thinning inks was utilized due to the different rheological response by the extent of physical stimulus such as shear stress.[20, 21] These fluids possessing self-standing and shape-memorable features have been classified as yield-stress fluids (or Bingham plastic fluids),[22-25] which is often observed in mayonnaise, ketchup, whipping cream, toothpaste, etc. They behave like a solid in the quiescent condition but flow like an ordinary liquid when a certain level of stress (i.e., yield stress) is applied.[26-28] For thermoset monomers, the yield-stress characteristics may be imposed by adopting hydrogen-bonding network in the fluids. The hydrogen-bonding network can lead to forming skeletal structures in thermoset monomers to maintain its shape against gravity, which is represented by the yield stress. This reversible self-assembly features of hydrogen-bonding can be used in the strategy of implementing yield-stress characteristics resulting in the phase transition between the liquid-like and solid-like states within several seconds.[29-32] Hydrogen bonding can be induced using functional groups between hydrogen attached to electrical negative atoms (e.g., N, O, F) and electron donator such as carbonyl oxygen (C=O). The self-assembled hydrogen-bonding skeletal structure allows the printed structure to maintain its shape against gravity, and simultaneously be crumbled with ease by an external shear force or agitation.[33] Accordingly, if this yield-stress capability is imposed to a high-performance thermosetting monomer, most likely epoxy resins, a novel 3D-printing feedstock can be developed, which can flow through the printing nozzle or connection tubes with ease at a very low viscosity, but behave like a solid immediately after being printed.[34-36]

As used in this study, epoxy resins are widely considered as one of low-viscosity(ca. 5-50 Pa·s) and high-performance thermosetting polymers used for a variety of engineering applications due to superior mechanical properties, thermal and dimensional stability, chemical resistance and ease of processing.[37-40] Particularly, it should be noted that the UV-curable acrylated (-CH2=CHCOO-) epoxy has both electron acceptors and donors for hydrogen bonding, corresponding to hydrogen (C-OH) and carbonyl oxygen (C=O), respectively, as schematically depicted in Fig. 1A. In order to induce a strong hydrogen-bond network, as used in this study (Fig. 1B), amides can be additionally used as an appropriate self-assembly agent because they contain both electron acceptors (NH) and donors (C=O) to form networks by itself as well as with epoxy acrylates, e.g., N-H··O=C. In the self-assembly agent, it is important to choose appropriate chain lengths and the equivalent molecular weight of NH, each influencing the speed and the strength of hydrogen-bond network. Comparing with other chemicals, we carefully selected octadodecylamide (ODA) as a self-assembly agent composed of 17 aliphatic -C-C- chains (ca. 2.4 nm) containing amide groups corresponding to an equivalent molecular weight of 141.7 g/eq, which is compatible with epoxy acrylate and exhibits the appropriate rheological behaviours under the printing condition exerting a strong yield-stress behaviour. This epoxy/self-assembly agent system can guarantee low-viscosity, UV-curable, and self-assembly characteristics as a yield-stress fluid, which subsequently makes it as an ideal 3D printing feedstock ensuring a versatile additive manufacturing.

In this paper, we propose a novel epoxy acrylate system including amide as a self-assembly agent exhibiting solid-liquid reversible responses ensuring the 3D continuous-filament printing. The rheological characteristics of the developed material was thoroughly investigated under static and dynamic conditions identifying the yield stress, viscosity, phase-transition speed, and allowable height of stacking. The self-standing and shape-memorable capability of the materials was clearly demonstrated by printing a stacked structure in the z-direction.

Experimental

Materials

A bisphenol A type epoxy diacrylate resin (EA) with 500 g/mol of the molecular weight and 2,4,6-trimethylbenzoyl diphenyl phosphinoxide (TPO) were purchased from ENTIS (South Korea). 1,6-hexanediol diacrylate (HDDA) and octadecanamide (ODA) were purchased from Sigma-Aldrich and Arkema, respectively. TPO was used as a photoinitiator, which has a maximum UV absorbance of 395 nm. HDDA and ODA were used as a diluent material and a self-assembly agent, respectively. Specially, comparing with our materials system, polydimethylsiloxane (PDMS) was used as a reference material that has a high viscosity (~10^5 Pa·s) without yield stress (purchased from TA Instruments, silicone standard #700.01011). As seen in Fig. 1, EA had potential hydrogen bond sites (O-H and C=O) and ODA three potential hydrogen bond sites (two N-H and one C=O). 30 g of EA was mixed with 10g of HDDA and vigorously stirred using a mechanical stirrer and 1 wt% of TPO was added. 1 wt% and 3 wt% of ODA were added to the neat EA, each corresponding to droplet and continuous-filament shape, respectively. Although not included here, the extrudate at 2 wt% of ODA exhibited a state in the middle of these two representative states at 1 and 3 wt%, and there was no significant change in the shape of extrudates when the ODA composition was over 3 wt%. Three different concentrations, 0, 1 and 3 wt% of ODA in the neat EA, were referred to as neat EA, EA/ODA1 and EA/ODA3, respectively, for the study of continuous-filament 3D printing.

Characterization

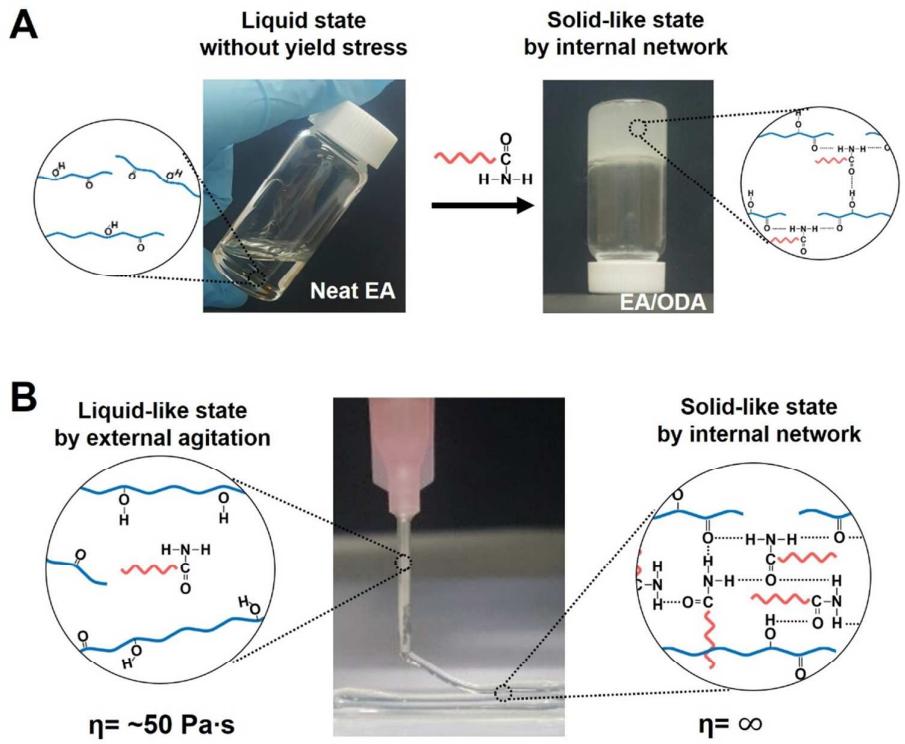

Fig. 1 Digital images of liquid state of neat EA and solid-like state of EA/ODA (A). The liquid state of EA is changed by adding ODA exhibiting two distinctively different states. EA and ODA are designed to form the intermolecular network structure by hydrogen-bond formation among the functional groups of EA and ODA molecules: (EA)=O···H-N-(ODA). EA/ODA behaves as the liquid-like state (η=50 Pa·s) flowing through the nozzle and the solid-like state (η=∞) after being printed on the substrate stacked layer-by-layer without being collapsed (B). Two different states of inks result from the level of applied shear rates or shear stresses.

The rheological characteristics were measured using a rotational rheometer (MCR 300, Physica, Germany) equipped with a parallel plate geometry (disk diameter: 20 mm, gap size: 1 mm). Flow sweep tests were carried out at shear rate from 10^{-2} to 10^{2} sec^{-1}. The dynamic oscillatory tests were performed as increasing the oscillation amplitude up to 100 % at a frequency of 1 Hz. A frequency sweep experiments (0.01-100 Hz) were performed at 1% strain. 3-step interval thixotropy experiments were conducted in three oscillation steps: the samples were subjected to a strain of 0.01%, subsequently a strain of 10% was applied and finally a step of 0.01% strain was implemented. The duration of each step was 60, 30 and 60 sec, respectively. All measurements were performed at 25°C. The optical images of extruded features were taken using a CCD camera.

Printing

The 3D printing machine (NP-expert, Enjet Inc.) employed in this study was designed to control the movement of the substrate stage in the X–Y axis and the nozzle in the Z-axis by a computer software. A micro-syringe pump (Harvard, new PHD UltraTMnanomite) was used to supply the prepared inks from a syringe (1 ml) into a stainless nozzle (21G: I.D. of 0.51 mm and O.D. of 0.80 mm). The flow rate was kept 15 µl/min. The detailed equipment and printing conditions were reported elsewhere.[39] To build up the 3-D structures, the nozzle is located on a desired position and the ink deposition is commenced by working the pump. After stacking one layer of a desired feature, the nozzle is raised up a constant height. When the final height is reached, the ink deposition is stopped and the nozzle is vertically lifted up in order to disconnect the 3-D printed structure.

Results and discussion

Fig. 2A shows liquid state of neat EA and solid-like state of EA/ODA, where ODA imparts yield stress to the neat EA to become a solid-like state due to the molecular skeletal structure through the hydrogen bonds. Low-viscosity neat EA flows toward tiling direction, while EA/ODA exhibits no flow against gravity force. Fig. 2B shows a state in the middle of printing, where EA/ODA is stacked in three layers. In this printing, the EA/ODA in shows two different stages each corresponding to liquid-like state inside the nozzle and solid-like state right after being printed in the stacked feature. When the ink is inside the nozzle, the shear rate or shear stress is applied to EA/ODA, which breaks the hydrogen-bonding network between ODA and EA molecules, resulting in a low-viscosity liquid at around ~50 Pa·s. After the ink being printed out of the nozzle, however, the molecular assembly quickly occurs to such an extent as to maintain filamentary feature, and the printed parts become a solid-like state at an infinity viscosity to maintain the shape of extruded filaments against gravity force.[40] It constitutes that EA/ODA exhibits typical behaviour of yield stress fluids caused by the molecular self-

assembly via hydrogen bonding. This liquid-solid transition of the ink could be quite advantageous as a 3D printing material offering a low viscosity ink inside the nozzle and an infinity viscosity extrudate constructing a self-standing 3D-printed structures. It facilitates that EA/ODA passes through the syringe nozzle and rapidly solidifies, which is referred to as a self-standing and shape-memorable capability.

Figs. 3A and 3B depict the apparent viscosity (η) and the shear stress (τ) as a function of shear rate ($\dot{\gamma}$) over 10^{-2}~10^{2} sec^{-1} comparing neat EA, EA/ODA1, EA/ODA3 and PDMS. In Fig. 3A, the viscosity of EA/ODA specimens (EA/ODA1 and EA/ODA3) is lower than that of PDMS, which is a reference material exhibiting a typical pseudoplastic behaviour, in the entire shear-rate range. Their viscosity continues to drop fast with increment of $\dot{\gamma}$, which is considered that our ink system is the thixotropic fluid exhibiting variable viscosity with respect to shear rate. For example, the viscosity of EA/ODA3 is decreased to ~10^{2} Pa·s, which is substantially lower than ~10^{4} Pa·s of PDMS both measured at 10 sec-1. It is clear that EA/ODA specimens are more advantageous than PDMS for printing through the fine nozzles due to their lower viscosity than PDMS. In the logarithmic plots τ vs. $\dot{\gamma}$ (Fig. 3B), the neat EA ink shows a typical Newtonian fluid behaviour exhibiting a linear increment of τ with $\dot{\gamma}$, and τ of PDMS is increased without a plateau region. On the other hand, τ of EA/ODA specimens clearly shows a typical yield-stress fluid behaviour exhibiting a constant τ with an increasement of $\dot{\gamma}$, which demonstrates the presence of "static yield stress (τ_y)," i.e., a shear-stress plateau as $\dot{\gamma}\rightarrow 0$.

Herein, the yield stress can be obtained by the extrapolation of shear stress to the zero shear rate region. Yield-stress fluids or Bingham fluids have been described by the Herschel-Bulkley model (H-B model) as follows:[41]

$$\tau = \tau_y + K\dot{\gamma}^n \quad (1)$$

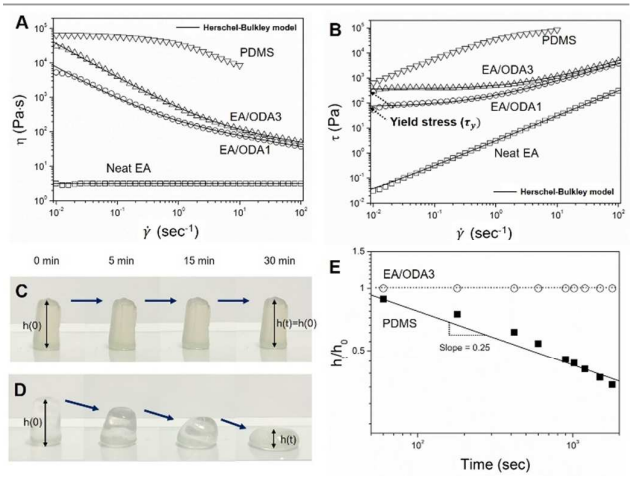

Fig. 3 The rheological characteristics of the neat EA, EA/ODA1, EA/ ODA 3 and PDMS: apparent viscosity (A) as functions of shear rate and shear stress (B) as function of shear rate compared with the Herschel-Bulkley model description (solid lines). Digital images extrudates of PDMS (C) and, EA/ODA3 (D), whose heights plotted as a function of time in (E).

where K is the consistency factor, and n is the flow behavior index. Analyzing the results in Fig. 3B based on Eq. (1), it can be seen that the H-B model compares well with the experimental results of neat EA and EA/ODA specimens with the model parameters summarized in Table 1. PDMS is not applicable for the H-B model. EA/ODA1 and EA/ODA3 give τ_y of 71.6 Pa and 364 Pa, respectively, which should be compared with that of 0 Pa for neat EA. When we assume that gravity is only applied to the printed structure of yield stress fluids, the structure can stand their own weight against gravity by the quantification of yield stress and their theoretical heights can be estimated, viz:[26]

$$h = \frac{\tau_y}{\rho g} \quad (2)$$

where h is the theoretical height, ρ is the density of the yield stress fluids and g is the acceleration of gravity. Using Eq. (2), h

Table 1 The parameters (τ_y, K, and n) of Herschel-Bulkly model, theoretical height (h) and dynamic yield stress ($\tau_{y,G}$) for neat EA, EA/ODA1 and EA/ODA3.

	τ_y (Pa)	K	n	h (cm)	$\tau_{y,G}$ (Pa)
Neat EA	0	3.13	0.999	0	-
EA/ODA1	71.6	138	0.714	0.6	40
EA/ODA3	364	150	0.746	3.2	210

of the extruded filaments of EA/ODA3 could be estimated as 3.2 cm, which is the visualized upright capacity corresponding to the yield stress (τ_y) of 364 Pa. It should be compared with the yield stresses of such materials as mayonnaise, ketchup and tooth paste corresponding to the yield stresses of 100, 30, and 215 Pa, respectively. In the other words, the extruded filaments can be overlaid repeatedly up to that height without spreading or collapsing by the gravity without any solidification steps. In practical printing processing, the overlaid structure is usually solidified *in-situ* by UV curing subsequently extending the theoretical heights of inks.

The yield-stress characteristics may be confirmed by observing the the extrudate shapes changing with time after being printed. In Figs. 3C and 3D, the height of PDMS, whose viscosity is much higher than EA/ODA, decreases by nearly 20% after 5 min. After 30 min, PDMS collapses by nearly 70%, spreading over the substrate. On the other hand, EA/ODA3 keeps its initial shape and height, where the spreading phenomena is not observed even after 30 min. Imposing yield-stress characteristics to EA, it demonstrates that the low-viscosity epoxy can be used as a feedstock of 3D continuous-filament printing device in a way of stacking the filaments just like high-viscosity thermoplastic polymers.

The gravitational spreading phenomena of a high-viscosity drop may be evaluated as a function of time assuming that a drop flows by the gravity force in the quasi-steady state:[42]

$$\frac{h_t}{h_0} = \frac{0.531}{h_0}\left(\frac{3vV}{gt}\right)^{1/4} \quad (3)$$

where h_t is the transient height, h_0 is the initial height, v is the kinematic viscosity, V is the volume of a drop, t is the time. Eq.

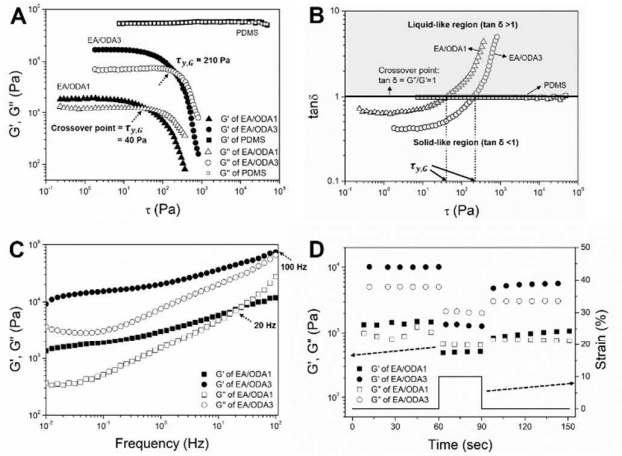

Fig. 4 Viscoelastic properties of EA/ODA1, EA/ODA3 and PDMS plotted by storage modulus, G', loss modulus, G", (A) and tan δ (B) as function of shear stress. G' and G" as a function of frequency (C) from 0.01 to 100 Hz under constant strain of 0.1% for EA/ODA specimens. The crossover point means the time scale of phase change between solid-like behavior and liquid-like behavior. G' and G" as a function of three time-steps at the applied strain in a low-high-low (0.01%-10%-0.01%) fashion using a frequency 1 Hz (D). The solid line represents the corresponding strain applied to the specimens.

(3) describes well the experimental results of PDMS as seen in Fig. 3E, where h_t decreases in proportion to $t^{-1/4}$. Compared with the collapsing PDMS, it is clearly seen that EA/ODA3, which is a yield-stress fluid, maintains the initial height against the gravity force regardless of time. It proves that EA/ODA3 exhibit the self-standing and shape-memorable capability that could substantially increase the printing speed and resolution by such a rapid stabilization of printed structures.

In this study, the phase transition of our ink systems between solid-like and liquid-like states are clearly demonstrated by analysing the viscoelastic properties each corresponding to storage modulus (G') and loss modulus (G") of materials. When G' is higher than G", the material is in a predominant solid-like state, and vice versa. In this sense, the crossover point of G' and G" can be attributed to the transition from the solid-like to the liquid-like states, which may very well correspond to the yield point of the material. In the oscillatory experiments, G' and G" of EA/ODA specimens and PDMS are plotted as a function of τ in Fig. 4A. EA/ODA1 and EA/ODA3 exhibit that G' is maintained higher than G" up to the crossover points of 40 Pa and 210 Pa, respectively, followed by the region, where G" is higher than G'. The obtained crossover points in Fig. 4A provide the dynamic yield stress ($\tau_{y,G}$) of EA/ODA1 and EA/ODA3, which agrees well with τ_y at 71.6 and 364 Pa in Table 1, respectively. When the ink flows through a nozzle, the wall shear stress in our experimental conditions can be estimated as 1825 Pa for EA/ODA3,[43,] which is higher than the yield stress ($\tau_{y,G}$ at 364 Pa) of our material. It supports that EA/ODA3 should flow in the liquid-like state inside nozzle at 50 Pa·s (Fig. 3A). However, when the ink is extruded out of the nozzle as filament, the applied shear stress becomes nearly zero, which it turns into a solid-like state. It can be further analysed using tan δ (G"/G'), which quantifies the elastic or viscous contributions by the borderline conditions of the phase transition at tan δ =1. Fig. 4B shows tan δ of EA/ODA specimens and PDMS as a function of τ. The tan δ of EA/ODA specimens increases with τ passing through the borderline at tan δ=1 representing a liquid-like behaviour in the low shear-stress region and a solid-like one in the high shear-stress region. It is clear that the shear stress at tan δ=1 consists with $\tau_{y,G}$ as measured in Fig. 4A. On the other hand, the tan δ of PDMS is 1.0 in the entire region. The time ($t_{y,G}$) required for the reversible liquid-to-solid transition may be evaluated by the frequency-sweep tests. Fig. 4C shows G' and G" of EA/ODA specimens measured as a function of frequency (f). The crossover points of EA/ODA1 and EA/ODA3 specimens are observed at f = 20 Hz and 100 Hz each corresponding to $t_{y,G}$=1/f = 0.01 sec and 0.05 sec, respectively. The crossover point of G' and G" is related with the phase transition, which may very well correspond to time required for the liquid-to-solid or solid-to-liquid transitions. This time may be ascribed to the time for EA and ODA molecules to form the skeletal network of hydrogen bonding. It should be associated with the time for the hydrogen bonding kinetics, viscosity and diffusion mobility of EA monomers and ODA, on the other hand, the hydrogen bond has a weak effect on the mechanical properties of our ink as seen in Fig. S1. Fig. 4D depicts the 3-step interval thixotropy test of EA/ODA specimens, which shows the typical characteristics of thixotropic fluids: the recovery of viscosity and/or moduli after the structure was broken down under the changing shear rates.[48] They exhibit G' higher than G" at a low strain at 0.01% but it turn vice versa at a high strain at 10%. When the low strain is applied again, the initial value of G' is rapidly increased and recovered. The first and last region (at low strain) shows the build-up of network structure and the middle region indicates the breakdown of the structure. This rapid and reversible response stems from the molecular self-assembly via hydrogen bonding allowing the breakdown or

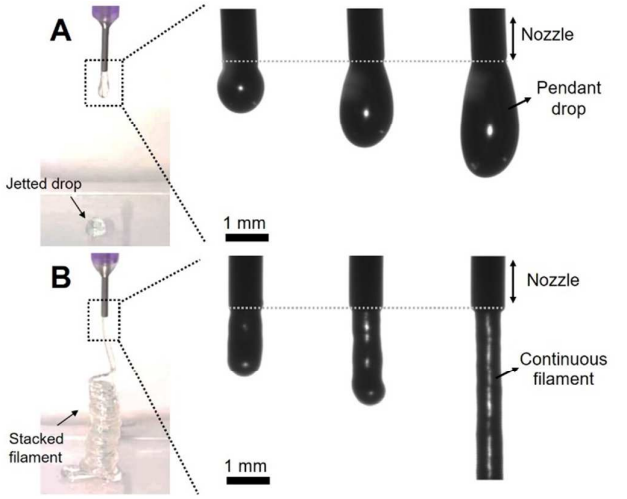

Fig. 5 Comparison of two different level yield-stress materials representing drop-jetting printing (A) and continuous-filament printing (B) each represented by sequential images of EA/ODA1 and EA/ODA3, respectively, extruded from the nozzle with inner diameter of 500 μm. Due to the low yield stress, EA/ODA1 has pendant drop, which is suitable for drop-jetting 3D printing. EA/ODA3 shows continuous filamentary shape due to high yield stress, which facilitates the filamentary features and endures the stacked layers

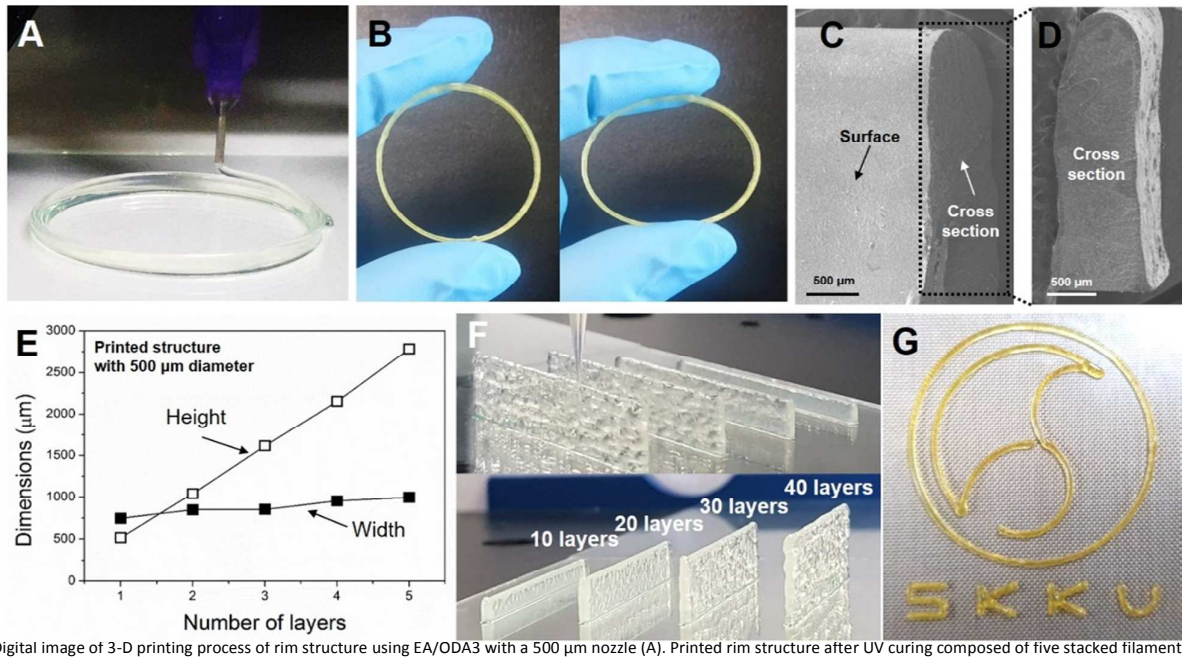

Fig. 6 Digital image of 3-D printing process of rim structure using EA/ODA3 with a 500 μm nozzle (A). Printed rim structure after UV curing composed of five stacked filament layers (B). SEM cross-section images of printed structure in side view in (C) and front-view in (D), the height and width of which are plotted in (E). Digital images of line structures with 10, 20, 30 and 40 layers (F) and 3-D printed gingko leaf structure (G), which is conducted using a tapered nozzle with a diameter of 200 μm.

reassembly of our ink system depending on the extent of deformation. In this regard, our inks have the reversible thixotropic nature, which is desired for 3D printing materials because they can easily flow through the nozzle and maintain the continuous-filament shape after extrusion.

Fig. 5 compares the sequential images of the low yield-stress ink (EA/ODA1) and high yield-stress ink (EA/ODA3) extruding out of the tip of the syringe needle. In general, as a spherical drop grows until the drop volume exceeds a critical weight for the drop to fall down. The maximum size of the drop held by the surface tension at the tip of the needle can be expressed by the following equation: $V_{max} = \sigma\pi D/\rho g$, where V_{max} is the maximum volume of the drop, σ is the surface tension of liquid and D is the diameter of the nozzle.[47] In yield-stress fluid, however, the yield stress (τ_y) is additionally exerted to hold the drop at the nozzle tip resulting in a drop in a long-neck pendent shape (Fig 5A), whose volume is bigger than V_{max}, or a continuous-filament shape (Fig. 5B) when the yield stress is further increased. Accordingly, it is clear that the yield stress is likely to be added to the intrinsic surface tension subsequently increasing the drop volume to surpass the gravity force resulting in the shape-memorable capability (retention of filamentary shape).

Using our high yield-stress ink (EA/ODA3), Fig. 6A demonstrates a stacked rim structure in a way of continuous-filament 3D printing. Due to high yield stress, the filaments are stacked with ease without buckling or spreading even before UV curing. When UV-cured (Fig. 6B), the printed rim structure turns yellow and becomes strong and robust maintaining its structural integrity even such a bending deformation. Figs. 6C and 6D show the cross sectional images of the 5-layer printed rim after UV curing. It indicates that no filamentary boundaries between individual printed filaments demonstrating that the interfaces of the printed layers are well cohered each other, which is the quite different from the printing cases of most thermoplastic materials. In thermoplastics, the overlaid boundaries often exhibit weld-lines leaving air pockets or week-interface lines due to the intrinsically-long relaxation time (or healing time) of high-molecular polymer chains. Fig. 6E shows the height and width of printed structures as a function of the stacking number of layers. The width is nearly constant, while their height is linearly increased. The thickness of each layer is 520 μm, which resultantly gives a structural height of 2.6 mm by stacking up only five filaments. To demonstrate the upright capacity of our high yield-stress ink (EA/ODA3), we printed a stacked wall structure (7.5 mm) composed of 40 stacked layers in a way of continuous-filament 3D printing as shown in Fig. 6F. Fig. 6G shows a printed symbol demonstrating the capability of our ink system printing complex patterns or shapes, e.g., a gingko-leaf feature, which is composed of multiple radii and sharp angles. It demonstrates that our material possesses the capability of building up 3D-printed self-standing structures without defects at the interfaces of stacked layers, which is attributed to the monomeric components of our ink system providing the superior mechanical properties of 3D-printed structures.

Conclusions

In this study, we developed a novel epoxy-based resin system, which has a shape-memorable and self-standing capability. The hydrogen-bond network was imposed by using an appropriate amide compound. Depending on the level of yield stress, the theoretical height of 3D printed structures could be predicted by theory and confirmed by experiments. The extrudate shape and spreading phenomena were identified

with time. Additionally, the tanδ accurately demonstrated the liquid-solid phase transition in the printing operating conditions. The yield stress and tan δ indicates that our high yield-stress fluid can be utilized by continuous-filament 3D printing, which would enable low-viscosity thermosetting polymers systems to exert the self-standing and shape-memorable capability.

Conflicts of interest

There are no conflicts to declare.

Acknowledgements

This work was supported by the National Research Foundation of Korea (NRF), the Ministry of Science, ICT & Future Planning (NRF-2014M3C1B2048175, 2016R1A2B1007134, and NRF-2017R1A2B4006091), and the Ministry of Trade, Industry and Energy (MOTIE) (10067690). We also appreciate the project and equipment support from Gyeonggi Province through the GRRC program of Sungkyunkwan University. KJK would like to acknowledge the partial financial support from the US National Science Foundation (#1545875).

Notes

J. D. Nam designed the experiments. H. Sun carried out the experiments and wrote the manuscripts. Y. Kim, Y. C. Kim and I. K. Park contributed to the data analysis. J. Suhr and D. Byun developed the overall concepts. K. Keon, O. H. Baek and Y. K. Jung provided coordination of the experiments. H. J. Choi and K. J. Kim conceived the idea. All the authors reviewed the manuscript.

References

1 B. C. Gross, J. L. Erkal, S. Y. Lockwood, C. Chen and D. M. Spence, *Analytical chemistry*, 2014, **86**, 3240-3253.
2 J. M. Zhang, E. Q. Li, A. A. Aguirre-Pablo and S. T. Thoroddsen, *RSC Advances*, 2016, **6**, 2793-2799.
3 Y. Jiang, Y. Chen, M. Zhang, Y. Qiu, Y. Lin and F. Pan, *RSC Advances*, 2016, **6**, 51871-51876.
4 K. Fu, Y. Yao, J. Dai and L. Hu, *Adv Mater*, 2017, **29**.
5 M. Faes, J. Vleugels, F. Vogeler and E. Ferraris, *CIRP Journal of Manufacturing Science and Technology*, 2016.
6 U. Kalsoom, P. N. Nesterenko and B. Paull, *RSC Advances*, 2016, **6**, 60355-60371.
7 Y. C. Kim, S. Hong, H. Sun, M. G. Kim, K. Choi, J. Cho, H. R. Choi, J. C. Koo, H. Moon and D. Byun, *European Polymer Journal*, 2017.
8 W. Jo, J. S. Lee, H. J. Lee and M.-W. Moon, *RSC Advances*, 2014, **4**, 31764-31770.
9 R. D. Farahani, M. Dube and D. Therriault, *Adv Mater*, 2016, **28**, 5794-5821.
10 1M. Zhang, A. Vora, W. Han, R. J. Wojtecki, H. Maune, A. B. A. Le, L. E. Thompson, G. M. McClelland, F. Ribet, A. C. Engler and A. Nelson, *Macromolecules*, 2015, **48**, 6482-6488.
11 P. Calvert, *Chemistry of Materials*, 2001, **13**, 3299-3305.
12 H. Lipson and M. Kurman, *Fabricated: The new world of 3D printing*, John Wiley & Sons, 2013.
13 N. P. Bansal and A. R. Boccaccini, *Ceramics and composites processing methods*, John Wiley & Sons, 2012.
14 X. Hao, J. Kaschta, X. Liu, Y. Pan and D. W. Schubert, *Polymer*, 2015, **80**, 38-45.
15 K. V. Wong and A. Hernandez, *ISRN Mechanical Engineering*, 2012, **2012**, 1-10.
16 A. Selimis, V. Mironov and M. Farsari, *Microelectronic Engineering*, 2015, **132**, 83-89.
17 J. Stringer and B. Derby, *Journal of the European Ceramic Society*, 2009, **29**, 913-918.
18 H. Sirringhaus, T. Kawase and R. Friend, *Mrs Bulletin*, 2001, **26**, 539-543.
19 C. J. Hansen, R. Saksena, D. B. Kolesky, J. J. Vericella, S. J. Kranz, G. P. Muldowney, K. T. Christensen and J. A. Lewis, *Adv Mater*, 2013, **25**, 96-102.
20 R. L. Truby and J. A. Lewis, *Nature*, 2016, **540**, 371-378.
21 M. Vatani, M. Vatani, J.-W. Choi and J.-W. Choi, *Rapid Prototyping Journal*, **2017**, 23, 337-343.
22 E. C. Bingham, *Fluidity and plasticity*, McGraw-Hill, 1922.
23 G. Benmouffok-Benbelkacem, F. Caton, C. Baravian and S. Skali-Lami, *Rheologica acta*, 2010, **49**, 305-314.
24 D. Bonn and M. M. Denn, *Science*, 2009, **324**, 1401-1402.
25 P. Moller, A. Fall, V. Chikkadi, D. Derks and D. Bonn, *Phil. Trans. R. Soc. A: Mathematical, Physical and Engineering Sciences*, 2009, **367**, 5139-5155.
26 H. A. Ardakani, E. Mitsoulis and S. G. Hatzikiriakos, *Journal of Non-Newtonian Fluid Mechanics*, 2011, **166**, 1262-1271.
27 H. A. Barnes, 2000.
28 P. C. F. Møller, J. Mewis and D. Bonn, *Soft Matter*, 2006, **2**, 274.
29 G. R. Desiraju, *Chemical Communications*, 1997, 1475-1482.
30 K. Wendler, J. Thar, S. Zahn and B. Kirchner, *The Journal of Physical Chemistry A*, 2010, **114**, 9529-9536.
31 J. A. Lewis and G. M. Gratson, *Materials today*, 2004, **7**, 32-39.
32 X. Zhou, C. Li, Y. Shao, C. Chen, Z. Yang and D. Liu, *Chemical Communications*, 2016, **52**, 10668-10671.
33 S. R. Raghavan, H. Walls and S. A. Khan, *Langmuir*, 2000, **16**, 7920-7930.
34 A. Abbadessa, M. Blokzijl, V. Mouser, P. Marica, J. Malda, W. Hennink and T. Vermonden, *Carbohydrate polymers*, 2016, **149**, 163-174.
35 G. M. Pawar, M. Koenigs, Z. Fahimi, M. Cox, I. K. Voets, H. M. Wyss and R. P. Sijbesma, *Biomacromolecules*, 2012, **13**, 3966-3976.
36 T. Billiet, M. Vandenhaute, J. Schelfhout, S. Van Vlierberghe and P. Dubruel, *Biomaterials*, 2012, **33**, 6020-6041.
37 N. Domun, H. Hadavinia, T. Zhang, T. Sainsbury, G. H. Liaghat and S. Vahid, *Nanoscale*, 2015, **7**, 10294-10329.
38 R. Thomas, D. Yumei, H. Yuelong, Y. Le, P. Moldenaers, Y. Weimin, T. Czigany and S. Thomas, *Polymer*, 2008, **49**, 278-294.
39 G. Pan, Z. Du, C. Zhang, C. Li, X. Yang and H. Li, *Polymer*, 2007, **48**, 3686-3693.
40 N. Chikhi, S. Fellahi and M. Bakar, *European Polymer Journal*, 2002, **38**, 251-264.
41 F. D. Prasetyo, H. T. Yudistira, V. D. Nguyen and D. Byun, *Journal of Micromechanics and Microengineering*, 2013, **23**, 095028.
42 P. Coussot, Q. D. Nguyen, H. T. Huynh and D. Bonn, *Phys Rev Lett*, 2002, **88**, 175501.
43 W. H. Herschel and R. Bulkley, *Colloid & Polymer Science*, 1926, **39**, 291-300.
44 S. Middleman, *An introduction to fluid dynamics: principles of analysis and design*, John Wiley & Sons Incorporated, 1998.
45 J.-F. Agassant, P. Avenas, P. J. Carreau, B. Vergnes and M. Vincent, *Polymer processing: principles and modeling*, Carl Hanser Verlag GmbH Co KG, 2017.

46 The wall stress in the Hargen-Poisueille equation is $\tau_w=\Delta PR/2L$. The experimental conditions of our printing are R=250 μm, ΔP=146,000 Pa and L=1 cm, which gives τ_w =1833 Pa.
47 J. Mewis and N. J. Wagner, *Advances in Colloid and Interface Science*, 2009, **147**, 214-227.
48 G. K. Batchelor, An introduction to fluid dynamics, Cambridge university press, 2000.

